

# Red and Yellow Traffic Lights Detection Robust to Various Lighting Conditions

Sorn Sooksatra\* and Toshiaki Kondo

Sirindorn International Institute of Technology, Thammasat University  
Rangsit Campus, Khlong Nueng, Khlong Luang, Pathum Thani 12120, Thailand

---

## Abstract

A traffic light is one of the most important traffic signs for drivers to drive smoothly and safely. However, drivers may fail to pay attention to it by some chance. Automatic traffic light detection may be a great help to cover driver's carelessness. This paper presents an automated traffic light detection method that works robustly under varying lighting conditions. We focus on the detection of red and yellow traffic lights because those signs are more crucial than green traffic lights for avoiding traffic accidents. The proposed method utilizes solely the color information in the CIELab color model, excluding the intensity information. The method is based on a simplified fast radial symmetry transform (FRST). The FRST is a fast implementation of the circular Hough transform. We also introduce a shape descriptor called solidity to reduce false traffic light detections. Simulation results show that the proposed method can significantly improve the precision and recall (sensitivity), that is, 79.19% and 87.5%, respectively, compared with conventional approaches.

**Keywords:** Traffic light detection; Fast Radial Symmetry; Computer Vision.

## 1. Introduction

Traffic light detection (TLD) is one of the most important issues in the advanced driver assistance systems (ADAS) that help to improve the safety of the car and passengers. In TLD, image processing and computer vision techniques are applied to digital images acquired by a digital camera installed in the vehicle. The TLD is generally based on some properties of traffic lights (TLs) such as their circular shape, colors, sizes, and the locations within the images. It is relevant to note that there are two structures of TLs; vertical and horizontal arrangements. In the vertical arrangement, the red light is located at the top, the yellow light in the middle, and the green light at the bottom as shown in Fig. 1(a). In the horizontal arrangement, on the other hand, the position of each color of a TL depends on the country where the TL is used. The red

light is located at the right in the countries where cars are driven on the left side of the road as shown in Fig. 1(b). Conversely, the red light is located at the left end in the countries where cars are driven on the right side of the road as shown in Fig. 1(c).

The detection of a green TL is considered less important as the driver needs no warning signal. Thus, the proposed method focuses on the detection of red and yellow TLs. The proposed method utilizes solely the color information in the CIELab color model, excluding the intensity information. The method is based on a simplified fast radial symmetry transform (FRST). The FRST is a fast version of the circular Hough transform. We also introduce a shape descriptor called solidity to reduce falsely detecting non-circular objects and also circular objects with a hole. Simulation results show that the proposed method

---

\*Correspondence : ohm.sorn@gmail.com

performs TLD robustly in various lighting conditions (both day and night times).

## 2. Related Work

As the advanced driver assistance systems (ADAS) have become more popular for several years, the researches on it are becoming more active. Let us briefly describe related works, especially on traffic light detection (TLD). It is common to use color information for TLD. There are a variety of color models. Normalized RGB signals are used for alleviating a negative impact on TLD from

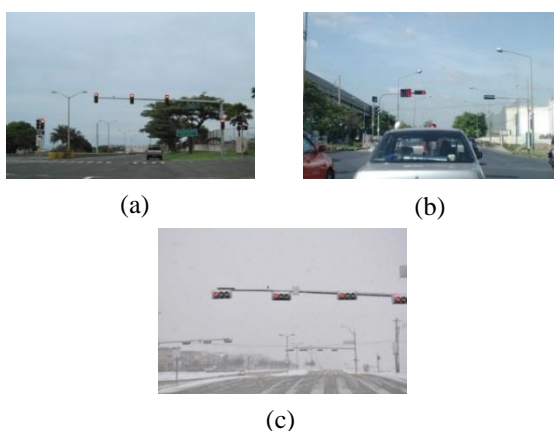


**Fig.1.** Different arrangements of traffic lights. (a) Vertical arrangement, (b) horizontal arrangement with the red light at the right end, and (c) horizontal arrangement with the red light at the left end.

varying lighting conditions, combined with a modified circular Hough transform in [1]. Normalized RGB signals are also used together with the dark surrounding structure of a TL to restrict regions of interest (ROI) further [2]. However, color and intensity information are not perfectly separated in the normalized RGB signals. As a result, their TLD performances are still dependent on changing lighting conditions. To cope with varying lighting conditions more robustly, other color models are utilized. For example, the Cb and Cr channels in YCbCr color model are used in [3], even though they

tested their method only on the images taken in the daytime. The CIELab and HSV color models also can be used for TLD since they essentially decouple color and intensity information. The CIELab model can be used for solving the blooming effect, that is, irregular intensity distribution on TL [4]. The HSV color model is used in [5], [6], and [7] where a Gaussian filter is used to emphasize TLs [5]. A database collected by [6] is used for classification by a support vector machine (SVM). The CAMSHIFT algorithm is used to track TLs in [7]. Ref. [8] describes a TLD technique that does not rely on color information. It uses the top-hat transform and the template matching technique with the correlation as the similarity metric.

Most researchers are concerned with only simple or general conditions about TLs. However, there are not many researchers who employ more specific features of TLs. There are some more research works that have been conducted, such as using an SVM for detecting TLs in night vision in [9], and an arrow-shaped TL using the Gabor wavelet transform and 2D independent component analysis (ICA) in [10].

## 3. Methodology

In the proposed research, we use the CIELab color model (as shown in Fig. 2) that was introduced by [11] and the fast radial symmetry transform (FRST) technique described in [4]. For detecting TLs, local maximum and minimum are used for detecting circular red and green TLs, respectively. For their extraction part, they use Eq. (1) from the CIELab color model.

$$ab = L \cdot (a^* + b^*) \quad (1)$$

where  $L$  is the luminance and  $a^*$  and  $b^*$  are the color components in the CIELab color respectively. As shown in Eq. (1), it is still sensitive to lighting conditions because  $L$  is involved in the equation. This can lower recall (sensitivity) and precision of the system under varying illuminations.

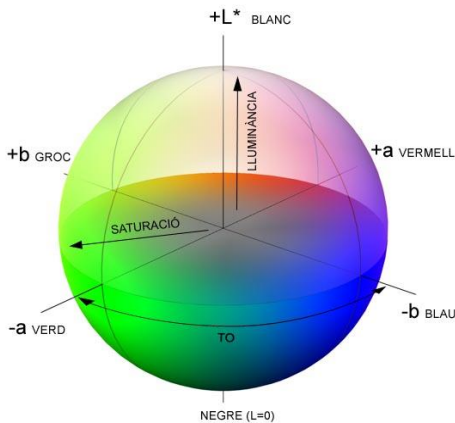


**Fig.2.** CIELab color model.

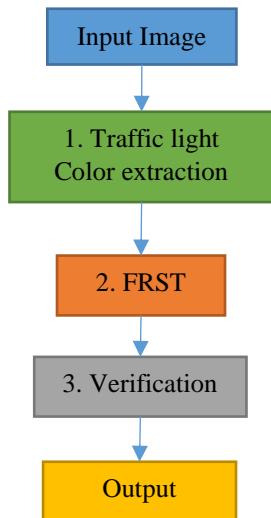


**Fig.3.** Flowchart of the proposed method.

To improve the research work from [4], we have modified some parts of their work and added a step for checking the shape of a detected object. We limit our target to only red and yellow TLs. This is because it is unnecessary to give a warning signal to a driver when the TL is green. As shown in Fig. 3, the proposed method comprises three steps. The first step is concerned with TL extraction using color information. The details of this step are described in Section 3.1. The second step, FRST, is implemented for detecting circular objects in an image.

The procedure of this step is explained in Section 3.2. The third step is designed for verifying TL extraction results using a shape descriptor. More details are given in Section 3.3. Since TLs are generally located at the upper half of the frame, we search for TLs only in the upper 55% of the image. In other words, the upper 55% of the image is our initial region-of-interest (ROI). The percentage, 55%, has been determined through experiments.

### 3.1. Traffic Light Extraction

In this step, we use only the  $a^*$  and  $b^*$  components of the CIELab color model for lighting conditions, not depending on the system. For extraction, red and yellow TLs should have high intensity in both  $a^*$  and  $b^*$  channels. In some cases, there is the blooming effect occurring in a red TL as shown in Fig. 4(a). To solve the problem, we propose to combine  $a^*$  channel (Fig. 4(b)) and  $b^*$  channel (Fig. 4(c)) to extract both of red and yellow TL in one channel by using Eq. (2). Then, the blooming effect can be removed as demonstrated in Fig. 4(d).

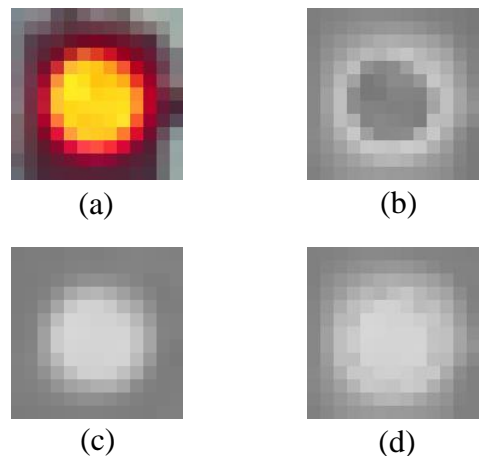


**Fig.4.** Blooming effect of a TL in (a) RGB image. (b)  $a^*$  channel, (c)  $b^*$  channel, and (d)  $ab^*$  image.

$$ab^* = \max(a^*, b^*) \quad (2)$$

Fig. 5(a) shows an input traffic image, while Fig. 5(b) shows the a-b channels of the input image. As shown in Fig. 5(b), a red TL has a high intensity in an input image. However, there are other objects with red or yellow color that also have high intensities. We next explain how to filter out those false targets.



**Fig.5.** Traffic light extraction result. (a) Input image, and (b) ab\* image.

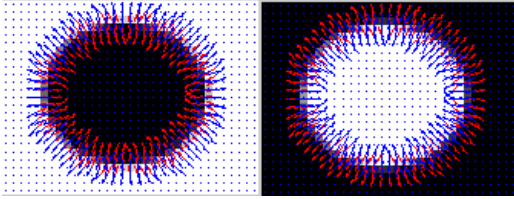


**Fig.6.** Positive (blue) and negative (red) gradient vectors on dark and bright circles.

### 3.2. Fast Radial Symmetry Transform

The fast radial symmetry transform (FRST) was proposed in [12]. It is used for detecting either bright or dark circular objects based on a given radius ( $r$ ). Since our target is circular TLs, we can use this technique to filter out the false targets detected in the preceding step.

This transform uses both directions (GD) and magnitudes (GM) of gradient vectors of an image. Every pixel in the image has its own gradient vector. We define a vector that points from a dark pixel to a brighter pixel as positive and otherwise negative. As shown in Fig. 6, we show positive vectors in blue and negative vectors in red. Those vectors can be computed using Eqs. (3) and (4).

$$(x_p, y_p) = (x, y) + \text{round}\left(r \frac{g(x, y)}{\|g(x, y)\|}\right) \quad (3)$$

$$(x_n, y_n) = (x, y) - \text{round}\left(r \frac{g(x, y)}{\|g(x, y)\|}\right) \quad (4)$$

where  $x_p, y_p$  and  $x_n, y_n$  are the coordinates in positive and negative directions, respectively.  $x, y$  are the coordinates of an input image and  $g(x, y)$  is the gradient of each pixel of the input image. With this gradient, we derive the orientation ( $O_r$ ) and the magnitude matrix ( $M_r$ ) for each radius ( $r$ ). They are initially zero matrices that have the same size as the input image. They are then updated using Eqs. (5) and (6). Then we can get the symmetry transform matrix ( $S_r$ ) by Eq. (7), where  $\alpha$  is the radial strictness parameter.

$$\left. \begin{aligned} O_r(x_p, y_p) &= O_r(x_p, y_p) + 1 \\ M_r(x_p, y_p) &= M_r(x_p, y_p) + \|g(x, y)\| \end{aligned} \right\} \quad (5)$$

$$\left. \begin{aligned} O_r(x_n, y_n) &= O_r(x_n, y_n) - 1 \\ M_r(x_n, y_n) &= M_r(x_n, y_n) - \|g(x, y)\| \end{aligned} \right\} \quad (6)$$

$$S_r = F_r * A_r \quad (7)$$

where  $F_r = \|O_r\|^\alpha \cdot M_r$  and  $A_r = 2\text{-D Gaussian}$ .

Eqs. (5), (6), and (7) are applied to every pixel in an image. Each pixel produces an array of vectors where those vectors are radially converged or diverged from the pixel.

The magnitude of  $S_r$  depends on the GM (Eq. (7)). For a circular object of radius  $r$ , both positive and negative vectors are presented radially from the center of the circle. Since we ignore regions with gradients of zero, these vectors appear only along the circle. Depending on the GD, either positive or negative, we accumulate a score positively or

negatively, resulting in positive and negative peaks in  $S_r$  (Eqs. (5), (6)).

Since the proposed method is concerned with the detection of only red and yellow TLs, the FRST can be modified by ignoring Eq. (6) to be a modified FRST (MFRST). Using the MFRST can reduce the computation time for this step. From input image (Fig. 7(a)) and  $ab^*$  image (Fig. 7(b)), it can be seen that red/yellow will have high height in the 3D-plot of MFRST as shown in Fig. 7(c) then exhibits the responses of the FRST, plotted in 3D. It is clear that the traffic light produces a prominent peak, from which the TL is detected as shown in Fig. 7(d). In addition, this technique can detect more than one radius at once by using Eq. (8), where  $N$  is the number of radii used. In the proposed method, we vary the radius from 1 to 15 pixels. The parameter space of the circular Hough transform is three dimensional which is spanned by  $x$ ,  $y$ , and  $r$ . Then, we perform maximum intensity projection. The parameter space of the circular Hough transform is three dimensional which is spanned by  $x$ ,  $y$ , and  $r$ . Then, we perform maximum intensity projection (MIP) vertically, namely, along the  $r$  axis, resulting in the 2D array,  $S$ . The MIP step is expressed in Eq. (8) and Fig. 7(c) shows a 3D plot of an  $S$ .

Meanwhile, we generate another 2D array,  $R$ , which shows the radius  $r$  of each entry of an  $S$ . For instance, if the first entry of  $S$  comes from  $S_{r1}$ , the first entry of new array  $R$  is  $S_{r1}$ . With the combination of  $S$  and  $R$ , we can locate circular objects with various radii in an input image as shown in Fig. 7(d).

$$S = \max(S_{r1}, S_{r2}, \dots, S_{rN}) \quad (8)$$

### 3.3. Verification

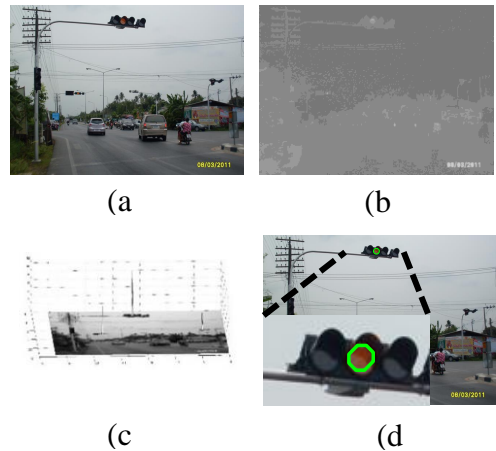
The MFRST tends to detect non-TLs as TLs, resulting in excessive false positives (FPs). This is because the technique cannot distinguish circular objects from ring-shaped objects. Round-shaped numbers and characters on a sign board are also often

detected as TLs. To reduce those FPs, we introduce ‘solidity’ that is described in [13]. Solidity describes the extent to which the shape of a pattern is convex or concave. It is defined by

$$\text{Solidity} = A/CA \quad (9)$$

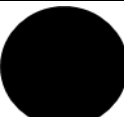





where  $A$  is area of the pattern and  $CA$  is the area of the convex hull of the pattern.

To demonstrate how the solidity works, Table 1 shows 3 patterns together with their convex hull areas and values of solidity. A circular pattern and its convex hull are similar to each other, namely,  $A=CA$  or  $A \approx CA$ , resulting in the solidity equal to or close to 1 (2nd column). Meanwhile, a donut-shaped pattern produces the solidity below 1 owing to the hole within the pattern (3rd column). A non-circular pattern also produces the solidity below 1 because of its irregularity in shape. In this manner, we may distinguish circular patterns from others.



**Fig.7.** Result of MFRST. (a) Input image, (b)  $ab^*$  image, (c) 3D plot of symmetry transform matrix  $S$ , and (d) detected using MFRST.

**Table1.** Examples of patterns with their convex hull area and solidity.

Pattern			
Convex hull area			
Solidity	1.00	0.74	0.82

#### 4. Results and Discussion

In this paper, we attempt to increase the precision and recall of the proposed method compared with those in [4]. In this section, we discuss about the proposed method based on simulation results.

##### 4.1 Orientation simulation test



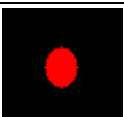
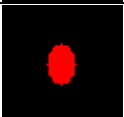
To find orientation or degree of TLs that can be detected, we create a circular object by using the ellipse equation in Eq. (10)

$$\frac{(x-x_c)^2}{a^2} + \frac{(y-y_c)^2}{b^2} = 1 \quad (10)$$

where  $x_c$  and  $y_c$  are the center of the circular object in  $x$  and  $y$  coordinate. In addition, 'a' and 'b' are major and minor axes, respectively.

We fix the value of 'a' to be 10 and vary 'b' in terms of the rate to 'a', namely,  $b/a$ , from 100 to 70% as shown in Table 2. The right-most column in Table 2 plots the peak height of each input pattern when the MFRST is applied. In the proposed method, we set the maximum peak threshold for detecting TLs to be 65. Table 2 shows that circular objects with the minor axis that is more than 80% of the major axis are still detectable. Therefore, the limitation of the orientation is 70 % of the major axis.

**Table2.** Orientation simulation result.

Rate b/a	Input image	Maximum Peak
100 %		129.9
90 %		127.72
80 %		68.11
70 %		33.56

##### 4.2 Lighting conditions simulation test

To evaluate the robustness of the proposed method to varying lighting conditions, we vary the intensities of an image in four levels as tabulated in Table 3. The pattern is a red circle of the fixed radius 10. Table 3 shows that the peak heights under the four different intensity levels are nearly constant. This indicates that the proposed method is robust to the changes in lighting conditions.

##### 4.3. Evaluation

We evaluate the performance of the proposed method using the statistical measures, precision, recall, and F1 score. When a traffic light (TL) is successfully detected, it is a true positive (TP). When a non-TL pattern is detected as a TL, it is a false positive (FP). When a TL is missed, it is a false negative (FN). Using these, the following statistics can be defined.

$$\text{Precision} = \frac{TP}{TP + FP} \times 100 \quad (11)$$

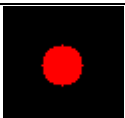



$$\text{Recall} = \frac{TP}{TP + FN} \times 100 \quad (12)$$



$$F1\text{-score} = \frac{2 \times \text{Precision} \times \text{Recall}}{\text{Precision} + \text{Recall}} \quad (13)$$

We use 100 street images that contain 200 TLs in total. We set the threshold to FRST at 65. The range of the radius is from 1 to 15 pixels. The threshold to the solidity is set at 0.85. The confusion tables and summaries of them are shown in Tables 4, 5 and 6.

**Table3.**Lighting conditions simulation result.

Intensity	Picture	Maximum Peak
1		129.9
0.8		129.1
0.6		129.91
0.4		120.15

**Table4.** Confusion table for the traditional method.

Real \ Detect as	Traffic lights	Non- Traffic lights
Traffic lights	TP = 118	FN = 82
Non- Traffic lights	FP = 118	

**Table5.** Confusion table for the proposed method.

Real \ Detect as	Traffic lights	Non- Traffic lights
Traffic lights	TP = 175	FN = 25
Non- Traffic lights	FP = 46	

Table 6 shows the percentage of the precision, recall, and F1 score in day time and at night by both traditional and proposed methods. It shows that the proposed method has higher scores in both daytime and night time, about a 30 % increase on average. As shown in Table 6, night time, which is 30% of our database, has a lower percentage than day time, especially for precision. It means that it has a lot of false positive at night. Therefore, this method has high successful rate in the day time.

Figs. 8 and 9 show successful TLD results by the proposed method. Fig. 8(a) shows TLD in a dark situation. There are two TLs in the input image, which are indicated by the two dashed-line rectangle boxes, A and B. They produce prominent peaks in the parameter space of the FRST as shown in Fig. 8(b). After thresholding to these peaks, the two TLs are detected successfully as shown in Fig. 8(c) and 8(d). Fig. 9 demonstrates that falsely detected TLs, i.e., false positives (FPs), are successfully rejected by the solidity. There is one TL in the input image in Fig. 9(a), which is encompassed by the dashed-line rectangle box A. There are numerous faulty peaks in the parameter space as shown in Fig. 9(b). These faulty peaks are rejected by the solidity, and only the TL is detected as shown in Fig. 9(c).

Figs. 10 and 11 show unsuccessful TLD results by the proposed method. Fig. 10(a) shows an input image at night, while Fig. 10(b) shows the 3D plot of the parameter space of the FRST. The region A in Fig. 10(a) contains a TL, which is correctly detected as shown in Fig. 10(c). Meanwhile, the region B in Fig. 10(a) has both TL and non-TL bright spots. For this particular case, the combination of the circular Hough transform and the solidity fail to distinguish non-TLs from true TLs as shown in Fig. 10(d). This shows an example of false positive (FP), which lowers the precision (Eq. (10)). Fig. 11(a) shows

**Table6.** Result of precision, recall, and F1-score.

Evaluation	Traditional method [4]			Proposed method		
	Day	Night	Total	Day	Night	Total
Precision	54.91%	36.51%	50.00%	85.55%	56.25%	79.19%
Recall	56.21%	74.19%	59.00%	87.57%	87.10%	87.50%
F1 score	55.56%	48.94%	54.13%	86.55%	68.35%	83.14%

another input image, while Fig. 11(b) illustrates the 3D plot of the parameter space of the FRST. The TL in box A in Fig. 11(a) is successfully detected as shown in Fig. 11(c). However, another TL located below box A is missed because of the region of interest (ROI) set earlier (Fig. 11(d)). This is an example of false negative (FN) that lowers the recall (Eq. (11)).

#### 4.4. Time Consumption

The proposed method is tested on an Intel Core i5 (2.8 GHz) processor with 8GB RAM. The resolution of an input full color image is the so-called QVGA, i.e., 240 by 320 pixels with 8-bit quantization levels for each of red, green, and blue colors. The proposed method is implemented using MATLAB R2009. For the time consumption, we compare the time consumption of the biggest part of this project, which is FRST, with traditional and proposed methods. The result is shown in Table 7.

**Table7.** Time complexity comparison.

FRST method	Traditional method (sec)	Proposed method (sec)
Mean	2.88	1.63
SD	0.24	0.10

Table 7 shows that the proposed method spends less computational time than the traditional [4], method because the proposed method has simplified the FRST by detecting bright spot (red and yellow TLs) only. Time consumption is reduced by about 55.82% of the traditional method. In addition, the proposed method has a more

stable time because it has lower standard deviations.

## 5. Conclusion and Future work

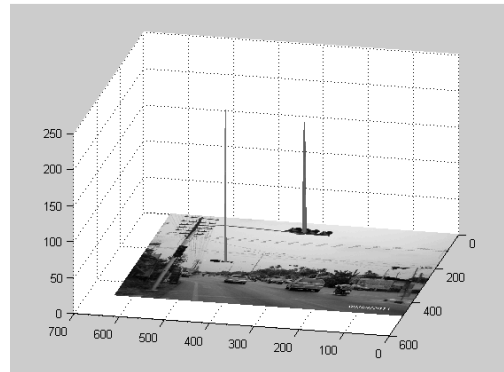
This paper presents a novel traffic light detection method that is robust to varying lighting conditions. The proposed method employs the CIELab color model. Unlike conventional methods, we make use of only the color information, namely, the  $a^*$  and  $b^*$  components in the model. Since the L component, that is, brightness, is excluded, the proposed method works regardless of the varying brightness of the scene. In addition, we have simplified the fast radial symmetry transform (FRST) by computing only in the positive gradient direction. Consequently, the computation of the proposed method is highly efficient.

As future work, we will work on the improvement of the precision of the proposed method by further reducing false positives (FPs), often caused by brake lamps. We also plan to test the method on real video sequences.





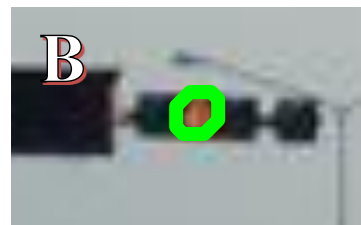
(a)



(b)



(c)

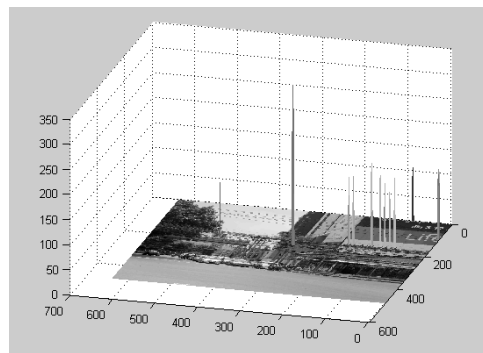


(d)

**Fig.8.** Traffic light detection in a dim environment. (a) Input image and result, (b) FRST 3D plot of (a), (c) cropped and enlarged region 'A' in (a), and (d) cropped and enlarged region 'B' in (a).



(a)



(b)

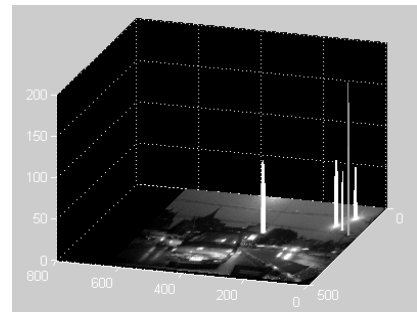


(c)

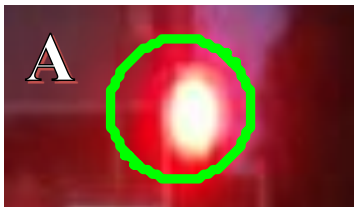
**Fig.9.** Traffic light detection with many false positives. (a) Input image and result, (b) FRST 3D plot of (a), (c) cropped and enlarged region 'A' in (a).



(a)



(b)

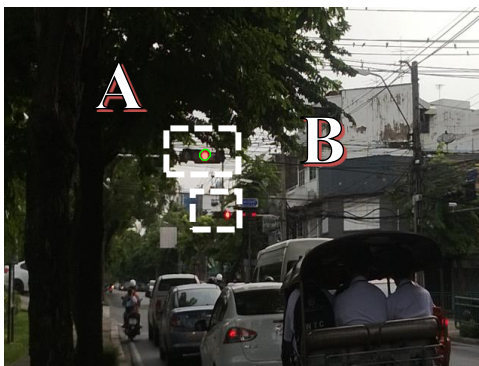


(c)

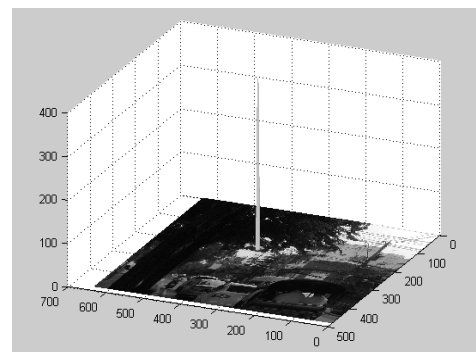


(d)

**Fig.10.** Detected TLs in a night scene. (a) Input image and result, (b) FRST 3D plot of (a), (c) cropped and enlarged region 'A' in (a), and (d) cropped and enlarged region 'B' in (a).



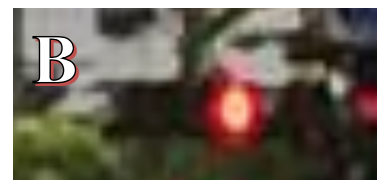
(a)



(b)



(c)



(d)

**Fig. 11.** Missed traffic light outside of the ROI. (a) Input image and result, (b) FRST 3D plot of (a), (c) cropped and enlarged region 'A' in (a), and (d) cropped and enlarged region 'B' in (a).

## 6. Acknowledgement

This research is financially supported by Thailand Advanced Institute of Science and Technology (TAIST), National Science and Technology Development Agency (NSTDA), Tokyo Institute of Technology, and Sirindhorn International Institute of Technology (SIIT), Thammasat University (TU) under the TAIST Tokyo Tech program. The information and some of pictures of TL in this research were obtained from the Bangkok Metropolitan Administration (BMA). Finally, the authors would like to express their gratitude to the anonymous reviewers for their constructive comments for significantly improving this paper.

## 7. References

- [1] Omachi M. and Omachi S., Traffic Light Detection with Color and Edge Information, *Computer Science and Information Technology 2nd (ICCSIT)*, pp. 284-287, 2009.
- [2] Moises Diaz-Cabrera, Pietro Cerri, and Javier Sanchez-Medina , Suspended Traffic Lights Detection and Distance Estimation Using Color Features, *Intelligent Transportation System 15th (ITSC)*, pp. 1315- 1320, 2012.
- [3] Hyun-Koo Kim, Ju H. Park, and Ho-Youl Jung , Effective Traffic Lights Recognition Method for Real Time Driving Assistance System in the Daytime, In *World Academy of Science, Engineering and Technology 59th*, 2011.
- [4] George Siogkas, Evangelos Skodras and Evangelos Dermatas , Traffic Lights Detection in Adverse Conditions Using Color, Symmetry and Spatiotemporal Information, *International Conference on Computer Vision Theory and Applications (VISAPP)*, pp. 620-627, 2012.
- [5] Yehu Shen, Umit Ozguner, Keith Redmill, and Jilin Liu , A Robust Video Based Traffic Light Detection Algorithm for Intelligent Vehicles, *Intelligent Vehicles Symposium*, pp. 521-526, 2009.
- [6] Cheng-Chin Chiang, Ming-Che Ho, Hong-Sheng Liao, Andi Pratama, and Wei-Cheng , Detecting and Recognizing Traffic Lights by Genetic Approximate Ellipse Detection and Spatial Texture Layouts, In *International Journal of Innovative Computing, Information and Control ICIC International*, vol. 7, pp. 6919-6934, 2011.
- [7] Jianwei Gong, Yanhua Jiang, Guangming Xiong, Chaohua Guan, Gang Tao and Huiyan Chen, The Recognition and Tracking of Traffic Lights Based on Color Segmentation and CAMSHIFT for Intelligent Vehicles, In *IEEE Intelligent Vehicles Symposium (IV)*, pp. 431-435, 2010.
- [8] Raoul de Charette and Fawzi Nashashibi, Real Time Visual Traffic Lights Recognition Based on Spot Light Detection and Adaptive Traffic Lights Templates, *Intelligent Vehicles Symposium* , pp. 358-363, 2009.
- [9] Hyun-Koo Kim, Young-Nam Shin, Sa-gong Kuk, Ju H. Park, and Ho-Youl Jung, Night-Time Traffic Light Detection Based On SVM with Geometric Moment Features, *World Academy of Science, Engineering and Technology 76th*, pp. 571-574, 2013.
- [10] Zixing Cai, Mingqin Gu, and Yi Li., Real-time Arrow Traffic Light Recognition System for Intelligent Vehicle, *International Conference on Image Processing, Computer Vision, and Pattern Recognition (ICCV)*, 2012.
- [11] X-rite, A Guide to Understanding Color Communication, pp. 12, 2007.
- [12] Loy, G., and Zelinsky, A., A Fast Radial Symmetry Transform for Detecting Points of Interest, in *Computer Vision—ECCV* , pp. 358-368, 2002.

- [13] Karuna G., Sujitha B., and Chandrasekhar Reddy P., An Efficient Representation of Shape for Object Recognition and Classification using Circular Shift Method, *International Journal of Scientific & Engineering Research*, Vol. 4, Issue 12, pp.703-707, 2013.